Gustafson, Paul Stuart

PHOSPHORUS-31 KNIGHT SHIFTS IN AMORPHOUS NICKEL-PHOSPHORUS AND NICKEL-COBALT-PHOSPHORUS ALLOYS

The College of William and Mary in Virginia PH.D. 1981

^{31}P KNIGHT SHIFTS IN AMORPHOUS NiP AND NiCoP ALLOYS

A Dissertation

Presented to

The Faculty of the Department of Physics

The College of William and Mary in Virginia

In Partial Fulfillment

Of the Requirements for the Degree of

Doctor of Philosophy

---

by

Paul Stuart Gustafson

1981

APPROVAL SHEET

This dissertation is submitted in partial fulfillment of the requirements for the degree of

Doctor of Philosophy.

Paul Stuart Gustafson

PAUL STUART GUSTAFSON

Approved, June 30, 1981

Dr. Harlan E. Schone, Chairman

Dr. J. W. Kossler

Dr. M. S. Conradi

Dr. Joe Heyman

Dr. G. C. Defotis,
Department of Chemistry

TABLE OF CONTENTS

DEDICATION iv

LIST OF TABLES v

LIST OF FIGURES vi

ABSTRACT ix

I. INTRODUCTION 2

II. EXPERIMENTAL PROCEDURE 9

A. Sample Preparation 9

B. Density 10

C. Composition Analysis 10

D. Spin Lattice Relaxation Times 11

E. Knight shifts 12

III. KNIGHT SHIFTS, THEORY IN TRANSITION METAL ALLOYS 14

A. Theory for Independent Bands 15

B. Anderson Virtual Band Model 21

C. Terakura's Hybrizied Band Theory, Fano Anti-Resonance 23

D. Negative Polarization; Core Polarization 26

E. Hybridized Transition Metal D Band Density of States . 28

F. Virtual D Band in the Hybridized Model 30

G. Amorphous Hybridized Band Model. 32

H. Linewidths, Spin Lattice Relaxation Time, and Korringa Ratio 37

IV. DATA AND DATA ANALYSIS 43
V. CONCLUSIONS 56

DEDICATION

To my family and friends, in thanks for their support and encouragement.

TABLES

Page

Table 1 Average nearest neighbor distance, R_{nn} measured to the first peak in the radial distribution function for electroplated $Ni_{100-x}P_x$, $Co_{78}P_{22}$ and splat cooled $(Ni_{.5}Pd_{.5})_{100-x}P_x$ amorphous alloys 58

Table 2 Atomic correlations from the partial radial distribution function for amorphous $Co_{78}P_{22}$ alloy, written as the radial distance r and number of near neighbors, n 59

Table 3 Atomic correlations from the partial radial distribution function for amorphous $Ni_{75}P_{25}$ alloy, written as the radial distance r and number of near neighbors, n 59

FIGURE CAPTIONS

Page

Figure 1 Radial distribution functions of: a) Ni-P(EP); b) Ni-P(EL); c) Fe-P-C (splat) from Cargill.[47] 60

Figure 2 Partial reduced radial distribution functions for $Co_{81}P_{19}$ 61

Figure 3 Partial radial distribution function for $Ni_{75}P_{25}$ . . 62

Figure 4 The Voronoi polyhedra or canonical holes of random packing: a) Archimedian antiprism shown capped by two half octahedra; b) trigonal prism capped by three half octahedra; c) tetragonal dodecahedron; d) tetrahedron; e) octahedron. 63

Figure 5 Block diagram of the NMR system 64

Figure 6 Compositional dependence of the low temperature magnetization of $Ni_{1-x}P_x$[48] 65

Figure 7 RKKY oscillations of free electrons about a local moment 66

Figure 8 Hybridized local DOS, N_L, calculated for a substutional impurity in FCC nickel, where V_0 = 0, 1.0 and 2.0 Rydberg. Full curves are the hybridized LDOS, broken curves are the unhybridized LDOS[37] . . . 67

Figure 9 Impurity local hybridized densities of state calculated from FCC in nickel a) weak potential; b) strong potential (Ref. 37) 68

Page

Figure 10 Dotted Curve: Local HDOS of substitutional impurity in Pd Full curve: Density of states in pure Pd; Broken curve: Schematic DOS of Pd in the presence of impurity atoms; E^{o}_{f} is Fermi energy in Pd; E'_{f} is Fermi energy in the presence of impurity atoms (Ref. 36) 69

Figure 11 The generalized phase shifts for various values of the impurity potential V_o. The deeper the potential, the greater the shift (Ref. 36). 70

Figure 12 Experimental partial DOS for amorphous $Pd_{81}Si_{19}$ from Riley, et al. (Ref. 43) 71

Figure 13 Theoretical PDOS for amorphous $Pd_{81}Si_{19}$ (Ref. 43). . 72

Figure 14 Broadening of the local d orbital DOS associated with an impurity of potential V_o (Ref. 36) 73

Figure 15 Schematic local valence electron HDOS near the d band edge for the $Ni_{1-x}P_x$ amorphous alloys. N_L for V_o = 1.0 Rydberg, N_L^+ for V_o = 1.1 Rydberg . . . 74

Figure 16 Exchange enhancement factor extrapolated from

$$S_d(E_f) = \frac{N_L(.925\text{Ryd.}) - N_o}{N_L(E_f) - N_o} \quad \ldots \ldots \ldots \ldots \ldots \ldots \quad 75$$

Figure 17 Modeled local susceptibilities χ_o high density, V_o = 1.0 Ryd. χ^+ low density V_o = 1.1 Ryd.. 76

Figure 18 Density of amorphous NiP and NiCoP alloys vs. phosphous concentration. △ EP (from Safranek, Ref.8); ○ El (Ref. 8); ▽EP (from Cargill, Ref.47); ◆ EL ◆ EP; ▲ EP $Ni_{71.7}Co_{8.3}P_{20}$; ● EL $Ni_{73.6}Co_{6.4}P_{20}$ . . 77

Page

Figure 19 ^{31}P Knight shifts of EL and EP $Ni_{1-x}P_x$ amorphous alloys vs. phosphorus concentration 78

Figure 20 ^{31}P NMR peak-to-peak linewidths, Δf_{pp}, of EL and EP $Ni_{1-x}P_x$ amorphous alloy vs. phosphorus concentration 79

Figure 21 Spin lattice relaxation times, T_1T, of EL and EP $Ni_{1-x}P_x$ amorphous alloy vs. phosphorus concentration 80

Figure 22 Korringa ratios of EL and EP $Ni_{1-x}P_x$ amorphous alloys vs. phosphorus concentration 81

Figure 23 Knight shift vs. cobalt concentration for amorphous EP $(Ni_{1-y}Co_y)_{80}P_{20}$ 82

Figure 24 NMR linewidth vs. cobalt concentration for amorphous EP $(Ni_{1-y}Co_y)_{80}P_{20}$ 83

Figure 25 ^{31}P Knight shift vs. cobalt concentration for EL $(Ni_{1-y}Co_y)_{80}P_{20}$ 84

Figure 26 NMR linewidth vs. cobalt concentration for EL $(Ni_{1-y}Co_y)_{80}P_{20}$ 85

Figure 27 Temperature dependent change in peak to peak linewidths vs. cobalt concentration 86

Figure 28 Knight shift vs. temperature for EL $Ni_{70.6}Co_{8.4}P_{21}$. 87

Figure 29 NMR linewidth vs. temperature for EL $Ni_{70.6}Co_{8.4}P_{21}$. 88

Figure 30 Knight shift vs. phosphorus concentration for EL $Ni_xCo_{6.0}P_y$ 89

Figure 31 NMR linewidths vs. phosphorus concentration for EL $Ni_xCo_{6.0}P_y$ 90

ABSTRACT

Amorphous alloys of the form $Ni_{1-x}P_x$ and $(Ni_{1-y}Co_y)_{1-x}P_x$ (where $.14 \leq x \leq .28$, and cobalt concentration is less than 13 percent) were prepared by electroplating (EP) and electroless deposition (EL). These two methods produce metallic glasses having different physical properties, indicating the existance of two metastable structures or phases. These phases were investigated by measurement of the ^{31}P Knight shifts, linewidths, spin lattice relaxation times and the physical densities. A comparison is made between the data and predictions of a hybridized band model which yields an expression for the enhanced local susceptibility at the phosphorus site.

^{31}P KNIGHT SHIFTS IN AMORPHOUS NiP AND NiCoP ALLOYS

I. INTRODUCTION

This thesis examines the NMR properties of $Ni_{1-x}P_x$ and $(Ni_{1-y}Co_y)_{1-x}P_x$ amorphous alloys, where the concentration of phosphorus is between 14 and 28 percent and the concentration of cobalt is less than 13 percent. One of the advantages of amorphous alloys is that experimental studies of concentration dependent phenomena may be expanded beyond the range of compositions determined by the crystalline phases. NiP and NiCoP amorphous alloys prepared by electroplating (EP) and electroless deposition (EL) have different physical properties, indicating the existance of different metastable structures or "phases". For example, $Ni_{81}P_{19}$ has room temperature Knight Shift values of K_{EP} = .158% and K_{EL} = .205% and a density difference of about 3% between the two phases.[1]

Nickel phosphorus is the oldest[2] and one of the most extensively studied metallic glasses forming an amorphous state in the composition range between 14 percent and 28 percent phosphorus. It is related to a group of metallic glasses commercially known as the Metglass series,[3] which have important engineering applications as brazing materials, specifically in the production of jet engine turbines.[4,5] In addition to ductility, important to this application, the isotropic, soft magnetic character of some of these alloys has potential for magnetic memories and other devices where easily changed magnetic orientation is desirable.

The interest in metallic glasses has a fundamental as well as a technological basis, as the properties of the alloys have forced a reappraisal of some of the traditional concepts of solid state physics.[6]

Amorphous alloys are metastable arrangements of atoms which are frozen into their positions. When subjected to moderately high temperatures the nucleation barriors of the material are breached, and the alloys crystallize through definite stages to the final stable ordered phase.[7] The only order present in the amorphous phase is short range, with the atoms densely packed in a semi-random pattern with fairly well defined first and second nearest neighbor distances. Beyond this level the order is rapidly lost, wiped out by the randomness of the amorphous structure.

Most metallic glasses have the general form $TM_{1-x}M_x$, where TM represents the transition metal (or metals), such as Fe, Co, Ni, Pd, or Pt, and M is the metalloid (or metalloids), such as B, C, P, or Si. The glasses can be prepared by a number of methods, including evaporation, sputtering, electroplating, electroless or chemical deposition and splat cooling. NiP and NiCoP may be formed by electroplating (EP) and electroless (EL) deposition. Each method produces an alloy with different characteristic physical density, with the EP materials having a higher density than the EL alloys for a given composition.[8]

Metallic glass structure can be discussed on at least two conceptual levels, the gross structural characteristics such as

density, voids, composition gradients, etc. and the more minute short range ordering (SRO) of the atoms in the material. By far the most useful description of the atomic arrangements can be found through the radial distribution function (RDF) of the atoms in the material. The RDF is just an average of the distribution of atoms in the material about an atom of origin, and is written as $RDF(r) = 4\pi r^2\rho(r)$. The atomic density distribution function, $\rho(r)$, is often presented in other ways, such as the reduced radial distribution function, $G(r) = 4\pi r(\rho(r)-\rho_0)$ or the pair correlation function, $W(r) = \rho(r)/\rho_0$, where ρ_0 is the average atomic density of the material. In a crystal the RDF would be a series of spikes of varying height located at the first, second, etc., nearest neighbor distances. In an amorphous solid the RDF is less precise, and has more similarities to the RDF's found for liquids than those seen for crystals.

RDF's may be obtained from X ray, electron and neutron scattering data by Fourier transformation of the measured momentum transfer dependent scattering intensity, I(K), and manipulating the expression to damp out the 'end' effect in the integral. Thus;[9]

$$G(r) = \frac{2}{\pi}\int_0^{\infty} K(I(K)-1)\sin(Kr)\,dK$$

and when damped becomes,

$$G(r) = \frac{2}{\pi}\int_0^{K_{max}} K(I(K)-1)e^{-bk^2}\sin(Kr)\,dK$$

The maxima in the RDF's correspond to the positions of the near neighbor atoms about the origin, and the intensity of those peaks roughly corresponds to the number of atoms contributing to the scattering. Many pure and binary metallic glasses have a doublet second maximum in the RDF, as seen in Fig. 1, which can be understood to be a result of the close packed structure of the material.[7] Information can be extracted from the RDF's in the form of the radial distances of the near neighbors, and the number and distribution of the neighbors.

Some amorphous binary alloys have been studied by X ray anomalous scattering techniques and by the polarized neutron scattering technique. These methods are able to separate the components of the RDF into the partial atomic distribution functions of the components of the alloy. The polarized neutron results for CoP,[10] shown in Fig. 2, and the X ray anomalous scattering results for NiP,[7] shown in Fig. 3, are quite similar. There appears to be no phosphorus-phosphorus nearest neighbors in these alloys, and each phosphorus atom has between eight and nine transition metal nearest neighbors. In addition the phosphorus-phosphorus nearest neighbor distance, R_{pp}, is nearly the same in both alloys. In CoP, R_{pp} = 3.34 Å and in NiP, R_{pp} = 3.30 Å.

Both EP and EL NiP alloys have been studied by X ray scattering, and the RDF's showed that the first nearest neighbor peak distances were about the same for either type of material.[11] The RDF results for NiP and some other amorphous alloys are displayed

in Table 1.[9] Note that the nearest neighbor distance, R_{nn}, in NiP is nearly constant through-out the range of composition, indicating a uniform structure is present in the EP materials. R_{nn} is primarily due to nickel-nickel scattering, and so does not yield information as significant as the results from the anomalous scattering method.

Many of the structural features extracted from RDF data can be observed in models based upon structures formed by dense random packing of hard spheres (DRPHS). Experiments with molded sacks of ball bearings and computer algorithums have been successful in showing distribution functions which agree quite well with the results from X ray RDF's. Distribution functions from densely packed single size ball bearings show the characteristic doublet second nearest neighbor peak, and have packing fractions similar to those found for amorphous samples. Finney,[12] Bennett,[13] Sadoc[14] and others have studied the 'atomic' arrangements which occur in these structures and have found that the whole structure can be considered to be built from only five different types of Voronoi polyhedra, or Bernal holes,[15] displayed in Fig. 4. Such modeling has only been done for single size ball bearings, but Polk[16] proposed a model for binary alloys in which the smaller size metalloids atoms occupy the voids in the polyhedral structure. The model has some difficulties handling the overall density and the limited volume in the voids simultaneously. The RDF data support the model to the extent that the metalloid atoms are surrounded by the larger transition metal atoms.[17] Sadoc proposed[14] that relaxation of the

polyhedral structure and the elimination of metalloid-metalloid nearest neighbors could be successfully modeled by a computer algorithum. The results of such computations closely match the NiP and CoP experimental RDF's and densities. In such models the metalloids occupy the interior of the polyhedral and have between eight and ten metal atom first nearest neighbors. Experimental data for NiP and CoP state that these alloys have between eight and nine metal nearest neighbors about each metalloid atom, in good agreement with the models.

With regards to both structure and stability, Bennett[18] and Turnbull[19] have suggested that the sharp repulsive potential of the transition metal atoms when combined with the softer metalloid potentials should enhance the stability of the material. Chen and Park[20] proposed that strong chemical, or ionic, bonding between the metal and metalloid atoms is the reason for the stability of these metallic glasses. Nagel and Tauc[21,22] suggested that the stability was due to a minimum in a nearly free electron-like density of states, and that the minimum was due to the nature of the amorphous state. The real nature of the bonding is uncertain, but almost no support has come forth for the free electron model of Nagel and Tauc, and little for the strong ionic bonding of Chen and Park. There is a possibility that covalent bonding occurs in some of the materials, but there are indications that some charge transfer, or ionic bonding, is present. It remains to be seen whether a more realistic model based upon replacement of the hard

spheres by 'pairwise potentials' can resolve some of the questions about bond order and stability in the amorphous alloys.[9]

II. EXPERIMENTAL PROCEDURE

A. Sample Preparation

Binary and ternary amorphous samples were prepared by electroplating from a modified Brenner bath[23] using direct current and electrodes of nickel and either a rotating or stationary copper substrate. The baths consisted of nickel (or nickel and cobalt) cloride and sulfate, phosphoric acid and phosphorous acid. The bath temperature was about 72°C, the pH was about .6 and the plating current density was about 10 amperes per square decimeter. Because cobalt has a higher ionic charge than nickel, only a small molar ratio of cobalt to nickel was needed in the bath to achieve substantial cobalt deposition in the plated alloy. Phosphorus deposition was increased by adding more phosphorous acid to the bath and by reducing the current density.

Electrolessly deposited alloys were prepared from Brenner's citric-acetic acid bath,[2] as this was found to be more stable and capable of greater phosphorus deposition than other baths. Nickel (or nickel and cobalt) cloride and sodium hypophosphite provided the other bath constituents.

For a given bath, the temperature and pH were held constant. The temperature range was between 70 and 80°C and the pH range was between 3.5 and 5.0. Cobalt was found to deposit at a slower rate

than nickel, requiring a high molar ratio of cobalt to nickel to achieve sufficient cobalt in the plated ternary samples. Baths with low temperatures and pH's produced alloys with high phosphorus concentrations. Production of high phosphorus concentration alloys was difficult as the bath would change as it aged, would slow and often stop the rate of deposition.

B. Density

In order to measure the physical density of the alloys, the copper substrate was removed in a chromic-hydrosulfuric acid etch which selectively disolved the copper and does not attack the more chemically resistant amorphous alloy.[8] The amorphous sample was weighed in air and deionized water on a "Gram-atic" balance[24] accurate to 10^{-4} grams. Repeated measurements of a sample weighing .5 grams showed a variation of less than ±1% in the measured density. The results of this process are shown in Fig. 18.

C. Composition Analysis

The compositions of the samples were determined by a non-destructive method using chemical analysis to determine the composition of standard samples then using a Princeton Applied Research X-ray flourescence analysis apparatus to determine the compositions of the remaining samples. The NiP sample was disolved in a hot nitric acid solution, the acid was neutralized and the phosphorus was precipitated from the solution by the addition of an ammonium-

molybdate solution. The weight of the cleaned, dried precipitate was then compared to the original sample weight to determine the phosphorus concentration. This procedure was repeated as an accuracy check. The above procedure has an accuracy of about ±1 percent phosphorus.[25]

With the assistance of Dr. S. Clement of the William and Mary Geology Department the remaining samples were analysed by comparing the measured intensity of the phosphorus Kα X-ray emissions of the unknown samples and the standards. The phosphorus composition of the unknown samples was then determined from a graph of Kα intensity versus phosphorus content of the standard samples.

The physical density of some of the flourescence analysed EP type samples was measured and compared to the known composition dependence of the density for EP NiP alloys.

The compositions from the density dependent measurements were within .2% of those aquired from the flourescence method. Thus, the listed sample compositions are believed to be accurate to within half a percent phosphorus.

In the ternary samples, the cobalt and nickel content was assumed to be directly proportional to the ratio of their measured Kα X-ray intensities.

D. Spin Lattice Relaxation Times

The relaxation times were measured for powder samples in a pulse NMR apparatus by a standard π, $\pi/2$ time delay method. The

The system was repeatedly pulsed and the output signal averaged. The magnitude of the magnetization was measured and graphed as the log of the magnetization vs. time, where the slope of the line was taken as the relaxation rate. The measurements were taken at room temperature and at a low temperature of either 150°K or 110°K.

E. Knight Shifts

The majority of the samples were measured at room temperature and at 77°K, and a few were also measured at 4°K. The NMR apparatus, shown diagramatically in Fig. 5, consisted of a lock-in amplifier, driving a field modulation coil and measuring the change in radio frequency power level of a tuned circuit (sample) in the magnet as the field is swept through the resonance. Most samples were measured with a marginal oscillator, which responds to the change in the tank circuit Q values as the sample absorbs energy when the field is swept through the resonance.

The output is amplified and then delivered to a signal averaging computer. For a field modulation amplitude of less than the resonance line width, the output appears as the derivative of the resonance line. By accumulating a number of sweeps, the signal to noise ratio improves as the signal adds coherently while the noise adds randomly.

One advantage of the above method is that the system measures resistance only, and, for samples of thickness less than the skin depth of the material, this system measures "χ", the

absorptive part of the effective susceptibility. As the samples were thin films on the order of 20 microns thick, and amorphous with poor conductivity, little or no eddy current mixing of χ' (dispersive) and χ'' (absorptive) is expected. The resistivity of $Ni_{80}P_{20}$ is about eighty times that of copper. Copper has a skin depth of about 20 microns at about 10 MHz,[26] therefore the skin depth of the NiP samples is much greater than the sample thickness.

The magnetic field was found to be homogeneous to less than half a gauss over a radius of about 2 cm at the sample position. The magnetic field at the sample site was checked before and after any series of measurements by measuring the ^{31}P resonance of a phosphoric acid reference.

III. KNIGHT SHIFTS, THEORY IN TRANSITION METAL ALLOYS

The observed nuclear magnetic resonance (NMR) frequency of a particular nucleus in a sample is displaced from that measured in a diamagnetic compound. This displacement is called the Knight shift after its discoverer, W. D. Knight.[27] For a given nuclear gyromagnetic ratio, the Knight shift is written as

$$f_0 = \gamma_n H_0 \quad \text{(diamagnetic)}$$

$$f' = \gamma_n (H_0 + \Delta H) \quad \text{(metallic)}$$

$$K = 100\left(\frac{f' - f_0}{f_0}\right) = 100\left(\frac{\Delta H}{H}\right)$$

$$= \text{Knight shift (in \%)}$$

The Knight shift samples the polarization of the conduction electrons in a metal because of the non-zero probability of such electrons at the nuclear site. The shift is often written as a function of the susceptibility and the nuclear coupling

$$K = (a)\chi$$

For a simple metal, the conduction electron susceptibility is directly related to the conduction electron density of states at the Fermi surface by $\chi = u_0^2 N_f(E_f)$, the Pauli susceptibility. The situation in transition metals and transition metal alloys is not so simple. The d bands dominate the band structure, and are

narrow and much higher than the conduction electron density of states. In the transition metals the d band density of state (DOS) dominates the magnetic character of the metal, even in the non-ferromagnetic region, as can be seen in Fig. 6. Analysis of NMR data can give some information about the structural electronic and magnetic properties of materials. In particular NMR analysis yields information about the local environment of the probe nuclei; their near neighbors, and the local susceptibilities and densities of states. Exact assessment of these physical properties from NMR data is difficult, but often NMR data serves as a way of testing and confirming results from other sources.

The following sections examine the terms present in the Knight shift and in particular, those terms which are pertinent to amorphous NiP and NiCoP alloys. The equation for the Knight Shift will be considered for the case of independent bands and then for the case of hybridization between the impurity (phosphorus) valence band and the transition metal d band. Also examined will be the responce of the d band to hybridization and change of impurity concentration and potential.

A. Theory for Independent Bands

The most commonly derived expression is the contact term which gives the shift due to non-interacting s electrons in a simple metal. It is generally written as:[28]

$$K_s = \frac{\Delta H}{H} = a_s \chi_s = \frac{8\pi}{3} \mu_0^2 \left|\psi_s(0)^2\right| N_s(E_f)$$

where:

a_s is the hyperfine coupling for the s electrons.

χ_s is the susceptibility for s electrons.

$\left|\psi_s(0)^2\right|$ is the probability of s electrons, of energy E_f, at the nuclear site ($r = 0$).

μ_0 is the Bohr marneton.

$N_s(E_f)$ is the density of s states as the fermi surface.

In general,

$$a_s = \frac{8\pi}{3} \left|\psi_s(0)^2\right| \quad \text{and} \quad \chi_s = \mu_0^2 N_s(E_f)$$

In addition to the contact term, the Knight shift also includes terms which couple to the contact term, and on occasion a spin dipolar term of other terms relating to the orbital character of the electron states. The dipolar term is anisotropic, but in an amorphous alloys would only contribute to the broadening of the resonance line, due to the isotropic character of the amorphous alloy.

There also exists a contribution due to the polarization of atomic-like closed s electron shells. These core states are polarized by non-s electrons through a spin interaction when polarized non-s electrons at the Fermi surface interact with the closed core levels. The interaction changes the contact probability of

the affected states such that $|\Psi^{+}_{core}(0)^2| - |\Psi^{-}_{core}(0)^2| \neq 0$, without changing the net polarization of the core levels. The core polarization term can be either positive or negative depending upon the type of electron responsible for the effect. While d states generally cause a negative polarization, p states can cause either positive or negative polarization. Although the data is incomplete, the change from negative to positive is thought to occur at about the $4p$ level.[28]

Further Knight shift terms can come from the diamagnetic susceptibility, the orbital or Van Vleck terms, and from spin and density oscillations of the conduction electrons from RKKY oscillations. Spin RKKY terms are generally due to the presence of a local moment which induces a radially oscillating spin response in the conduction electrons. Density RKKY terms come from the introduction of an impurity which draws or excludes conduction electrons and so induces a radailly oscillating conduction electron charge density. In most cases only a few of these terms might apply, but a complete expression for the Knight shift would be:

$$K = K_s + K_p + K_d + K_{vv} + K_{orb.} + K_{dia}$$

where in the presence of a local moment the conduction electron term becomes, $K_{s,RKKY}$.

In the literature, K_d and K_p often represent not only the core polarization terms, but also the conduction band response to

the s-d admixture.[26,28] In this discussion they will only represent the core polarization, all additional conduction electron polarization will be absorbed into K_s.

The above terms are for independent bands of non-interacting electrons, however, in transition metals the d band dominates the electron structure and in particular, there is a strong d-d exchange interaction which enters into the magnetic behavior. If the susceptibility is written to include this interaction, then the Stoner formula for the susceptibility of the d band is written as:[30]

$$\chi_d = \frac{\mu_0^2 N_d(E_f)}{(1 - U_{dd} N_d(E_f))} = \mu_0^2 S_d(E_f) N_d(E_f)$$

where U_{dd} is the d-d interaction strength and S_d is known as the Stoner enhancement factor. The Stoner enhancement factor represents the additional splitting of the up and down spin bands due to the electron-electron interaction and is a very significant term in the transition metals. Note that the transition from paramagnetic to ferromagnetic behavior occurs when $(1 - U_{dd}N_d(E_f)) = 0$, that is, when the enhancement factor becomes infinite. Electron-electron enhancement is also present for the s and p electron bands, but the interaction strength is small and they effectively act as free electrons. Often the s and p electrons are mixed in the conduction band, and in this paper this band will be referred to as the valence band.

For phosphorus, one expects the majority of the electrons at the Fermi surface to be p-like but, since the nuclear coupling for s electrons is so much greater than that for p electrons, even a small s electron density can strongly contribute to the valence band Knight shift. To simplify the discussion, it has been assumed that the nuclear coupling terms can be taken as constants throughout the composition range of the samples.

The orbital, Van Vleck and diamagnetic terms are important in some materials, but should not contribute significantly in NiP and NiCoP metallic glasses. The first two terms are largest for half filled d bands, and since the d bands in these alloys are nearly filled, these terms can be ignored.[29] The diamagnetic shift is important in metals such as beryllium and bismuth[26] but should be very small in these alloys. A later section shows that the K_p and K_d core polarization terms can be ignored since the polarization of the phosphorus core levels is much smaller than the contact term.

The terms due to RKKY charge density oscillations are less important in bulk alloys than in dilute systems, and can be ignored. The RKKY term due to the presence of local moments in the material cannot be so easily discarded. Many of the alloys have compositions very close to the ferromagnetic transition point (FMTP) and so the probability of local moment formation is high. A local moment produces a polarization density distribution, with the magnitude determined by the strength of the local moment, and the spacial development proportional to:[30]

$$\frac{\delta\rho_\sigma}{\rho_o} \propto \frac{x\cos(x) + \sin(x)}{x^4}$$

where $x = 2k_f R$. For large distances this may be written as:

$$\frac{\delta\rho_\sigma}{\rho_o} \propto \frac{\cos(2k_f R + \eta_l)\sin(\eta_l)}{R^3}$$

where η_l is a phase shift.

The oscillating polarization density has both positive and negative contribution, but the initial nearest neighbor contribution dominates due to the R^{-3} dependence of the field. This contribution to the Knight shift is negative for almost all materials, as seen in Fig. 7, and the spin field then has an average negative contribution to the Knight shift. The spin field also causes broadening of the linewidth. Both the change in the Knight shift and the linewidth are temperature dependent, following the temperature dependence of the strength of the local moment and increasing as the temperature is reduced.[31]

The expression for the Knight shift has been reduced to either the contact term, K_s, or the contact term modified by the presence of local moments, $K_{s,RKKY}$. The contact term has absorbed the extra polarization due to s-d hybridization.

In the following sections the valence band will be examined for the case of interacting bands by use of a hybridized band theory, and it will allow a much clearer understanding of the probable electronic structure of the amorphous alloys.

B. Anderson Virtual Band Model

Anderson[32] derived an expression for the polarization of the conduction band in the presence of a resonant d state. With this Anderson was able to derive the Anderson-Clogston Compensation Theorem, which showed that the local moment did not additionally polarize the conduction band. However, he did not examine the possible polarization when the moment was not formed. The equations which follow show the result of such as examination.

By use of approximations, Anderson showed that the conduction band response to the resonant d state may be written as:

$$\rho_{\sigma}(E) = \rho_0(E) + \frac{d\rho}{dE}\frac{|V_{dk}^2|(E-E_{\sigma})}{(E-E_{\sigma})^2+\Gamma^2}$$

where

E_{σ} is the energy of the virtual d state.

V_{dk} is the s-d admixture matrix element.

$\Gamma = \pi |V_{sd}|^2 \rho_s(E)$ represents the lifetime broadening of the d state due to the admixture, V_{sd}, between the d state and the conduction band, $\rho(E)$.

The total number of electrons of a given spin is:

$$N_{\sigma}^{\sigma} = \int_{-\infty}^{E_F} \rho_{\sigma}^{\sigma}(E)\,dE$$

It is obvious that the $\rho_0(E)$ term simply yields the normal Pauli susceptibility, the second term is:

$$\Delta N_f^{\sigma} = |V_{sd}^2| \int_{-\infty}^{E_f} dE \, \frac{d\rho(E)}{dE} \, \frac{(E - E_{\sigma})}{(E - E_{\sigma})^2 + \Gamma^2}$$

Anderson solves for the polarization for the local moment case and finds:

$$\Delta M = N_f^{+} - N_f^{-} = \ln \left| \frac{(E_f - E_+)^2 + \Gamma^2}{(E_f - E_-)^2 + \Gamma^2} \right|$$

since $|E_f - E_+| = |E_- - E_f|$ for the local moment case.

If the d state does not form a local moment, then the above condition is not satisfied. In the presence of an external magnetic field the d state energies become: $E_+ = E^0 - \delta E$ and $E_- = E^0 + \delta E$, where $\delta E = \mu_0 H S_d$.[33] With this, the polarization integral, for small δE, becomes:

$$\Delta M = |V_{sd}^2| \int_{-\infty}^{E_f} dE \, \frac{d\rho(E)}{dE} \, \frac{2\delta E}{(E - E^0)^2 + \Gamma^2}$$

Thus the susceptibility has the form[34]

$$\chi = \chi_{Pauli} + \mu_0^2 S_d I$$

where I is the integral or summation of the conduction band response to the admixture with the d state.

The integral term, I, must be in the form of a state density, and from the derivation it should represent the change in the conduction electron density of states due to s-d hybridization. Because of Anderson's evaluation technique, the integral term lacks some terms which would be present in a more exact derivation. The next section examines a more rigorous approach to the problem of hybridization in transition metal alloys.

C. Terakura's Hybridized Band Theory, Fano Anti-Resonance

The correlation between Terakura's equations and those from the Anderson model is close. Both start with the same Green's function, but Terakura's derivation[36] is more exact than Anderson's. The mechanics of this derivation may be found in reference 35. The local density of states at the non-transition metal site is shown by Terakura to be:

$$N_L(E) = N_0(E) + \frac{1}{\pi} \frac{A^2\Gamma + 2AB(E - E_d - \Delta) + B^2\Gamma}{(E - E_d - \Delta)^2 + \Gamma^2}$$

where

$\Gamma = \pi \sum_k |V_{dk}|^2 \delta_{E,E_k}$ is the width function

$\Delta = \mathcal{P} \sum_k |V_{dk}|^2 / E - E_k$ is the energy shift

N_0 is the original density of states (DOS)

N_1 is the hybridized DOS

E_d is the energy eigenvalue of the d states, and where A and B are the real and imaginary parts resulting from summation over the Green's function by k and k' (The initial and final conduction electron states).

The hybridized band equation may be written as:

$$N_L/N_0 = 1 - u - u\,\frac{(E - E_d - \Delta + (A/B)\Gamma)^2}{(E - E_d - \Delta)^2 + \Gamma^2}$$

where $U = B^2/\pi\Gamma N_0(E)$, and by substituting $\varepsilon = (E - E_d - \Delta)/\Gamma$ and $q = A/B$ it becomes:

$$N_L/N_0 = 1 - u - u\,\frac{(q + \varepsilon)^2}{\varepsilon^2 + 1}$$

The last term in the above equation is in the form of a Fano anti-resonance.[36] An anti-resonance shifts states from the position of the anti-resonance to higher and lower energies. Since the second term in the first equation is solely a function of the energy of the d state, it is simple to show that the derived susceptibility from Terakura's equations is of the Anderson form:

$$\chi_L = \chi_0 + \mu_0^2 S_d I = \chi_0 + \mu_0^2 S_d \left(N_L(E_f) - N_0(E_f)\right)$$

Anderson's integral has been replaced by the difference between the new hybridized band, DOS, calculated from the summations of the terms in the second equation, and that for the original unhybridized valance band. As would be expected, the change in the density of states shifts with the d band density of states and so responds to the magnetic field with the same enhancement factor as that of the d states. In a later paper[37] Terakura derives an equivalent expression for the susceptibility by a more complicated

procedure and finds:

$$\gamma_L = \mu_0^2 N_L(E_f) + (\alpha - 1)\bar{S}_L(E_f)$$

$$\text{where } \alpha = S_d(E_f) \text{ and } \bar{S}_L(E_f) = N_L(E_f) - N_0(E_f)$$

It is important to note that the enhanced term is the difference between the hybridized and original density of states, and that this term may be either positive or negative. If the d band enhancement factor, (either $S_d(E_f)$ or α) is large, and the enhanced term negative, then the polarization of the valence electrons could be large and negative.

In order to explore the facets of the theory, Terakura has done numerical calculations to dind the hybridized density of states of an impurity by use of a cluster representation for the transition metal atoms surrounding the impurity.[36,37] The impurity was represented by a square well potential of depth V_0 and radius 'a', the unhybridized densities of states and wave functions for both the square well and the metal atoms were determined and the effects of the hybridization were calculated. This generates the values for $\Delta(E)$, $\Gamma(E)$ and $q(E)$, which then allows one to calculate the hybridized valence band DOS. Terakura's diagrams, seen in Fig. 8, show how $N_L(E)$ varies as a function of the impurity potential or an impurity surrounded by twelve nickel atoms, which corresponds to a first nearest neighbor cluster of a FCC lattice. It is interesting to note that the 'dip' or anti-resonance position is located

at $E_a = E_d + \Delta(E) - q(E)\Gamma(E)$ and the upper peak in the hybridized valence band is located at $E_p = E_d + \Delta(E) + \Gamma(E)/q(E)$. Note that the dip position is nearly independent of the potential of the impurity, and that the hybridized band peak rises and shifts toward the d band as the potential of the impurity is increased.

Since Terakura's calculations are for clusters of nickel about an impurity, which is similar to the structural character of amorphous NiP, some conclusions about the probable form of a model for the alloys might be made. The next section will discuss core polarization, and the effects of hybridization upon the transition metal d band and the position of the Fermi level.

D. Negative Polarization; Core Polarization

It was stated that it was unlikely that a large core polarization term was present in the NiP amorphous alloys. The previous sections indicated that the enhanced susceptibility equation was capable of accounting for a strongly enhanced negative polarization of the conduction band, if the impurity potential was weak enough to allow the differnece between the hybridized and original densities of states to be negative in the presence of a strong enhancement term.

Figure 9 shows that for a strong impurity potential, $\overline{S_L}(E_f)$ is positive and for a weak potential $\overline{S_L}(E_f)$ is negative. If the diagram in Fig. 9a represented the hybridized impurity band of dilute silver in palladium, then, for an exchange enhancement factor

$S_d(E_f) = 8.0$, (nearly that of pure palladium), and for a density of states difference of $\overline{S_L}(E_f) = -0.5N_0(E_f)_{0+}$, the Knight shift would be about -1.566%. This value is near the experimental value of -1.5% for an alloy of 1.0% silver in palladium.[26] Furthermore, if the Fermi level were to rise as the impurity concentration increased, then $\mathcal{A}$ and K would rise until they reached the values for the pure metal as the Fermi energy mapped out both the enhancement factor and $\overline{S_L}(E_f)$. Thus the composition dependent Knight shift would have the appearence of a core polarization, but negative conduction electron polarization caused by the hybridization gives a more complete explanation.

It is pertinent to note that negative Knight shifts of this form only appear to take place for low valence atoms such as hydrogen, silver and copper, when they act as dilute impurities in palladium.[26] Higher valence atoms such as aluminum do not show the strong negative Knight shifts seen in the low valence impurities.[26] It would seem that the negative Knight shifts are nicely explained for the case of shallow impurity potentials in transition metal alloys.

Freeman and Watson[38] have shown that for an iron atom, the core polarization caused by an unpaired 4s electron is about one tenth the size of the direct contact term. Katayama, et al.,[39,40] have considered the difference between hyperfine fields (H_{hf}) caused by the local hybridized density of states and that likely to occur due to core polarization. For the case of high valance impurity atoms

in nickel metal, they conclude that "the direct Fermi contact interaction is responsible for the systematic variation of H_{hf}".[39] This coupled with the analysis of the model leads to the conclusion that only small core polarization terms are present in these alloys.

The earlier mention of a rising Fermi level mapping out the density of states and the enhancement factor was linked to a concentration change in the alloys. The response of the d band to hybridization and rising impurity concentration is the subject of the following sections.

E. Hybridized Transition Metal D Band Density of States

A model developed by K. Terakura can allow some understanding of the change of the transition metal d bands upon alloying. There are two essential concepts, that the d band is broadened and some number of d states are shifted to higher energies by the hybridization, and that for covalent bonding, that is, no charge transfer, the d band floats in relation to the Fermi energy in such a way as to conserve the number of d 'holes' per atoms for the transition metal element. Thus the d band appears to sink below the Fermi level, but actually maintains the same number of empty d states above the Fermi energy. The appearence of this condition, seen in Fig.10, is the same as if the Fermi level were rising as the d band were filled.

Terakura has calculated this effect using a cluster model, determining the generalized phase shifts of the transition metal

d states as a function of impurity potential. The upward shift of the hybridized d states caused by the phase shifts changes with the impurity potential, deeper potentials increase the phase shift term which induces more d states to shift to higher energies, as can be seen in Fig. 11. This is consistent with the concentration dependence of the ferromagnetic transition points found for NiP NiSi and NiAl[42] that is, as the valence increases, the concentration of metalloid necessary to destroy ferromagnetism decreases. Increasing the concentration of the impurity increases the number of d states affected by the hybridization, and thus changes the d band density of states at the Fermi surface. By shifting d states to higher energies, the Fermi level is also changed. Even for the case of no charge transfer the Fermi level must move to higher energies to insure the correct amount of band filling. Increasing either the concentration or valence of the impurities causes the Fermi energy to sweep upward in energy through the density of states. The d band density of states at the Fermi energy changes rapidly, and the enhancement factor, S_d, which is a function of $N_d(E_f)$, and U_{dd} changes even more rapidly as the nickel atoms become more dilute. It is intersting to note that if charge is transfered from metalloid to transition metal then the process is similar, but the Fermi energy sweeps even more rapidly through the density of states.

The hybridized valence band density of states is primarily determined by the impurity atom's relationship to its nearest

neighbors. The situation for amorphous alloys is unique in this instance, since the concentration does not necessarily change the structure of the material or the appearance of the hybridized valence band. Crystalline alloys have predetermined bond order, and concentration changes can mean a change in phase, and thus a change in structure.

Support for this picture of the transition metal alloy band structure can be found from the XPS, UPS and auger experiments performed by Riley, et al., upon amorphous $Pd_{81}Si_{19}$[43]. The experimental data was analysed so as to separate the Pd and Si contributions and thus achieve a picture of the Pd and Si densities of states. The graphs in Fig.12 clearly show the bonding and antibonding states characteristics of the hybridized band theory, and the Pd d band, smoothed by loss of long range order and narrowed by dilution. The Fermi energy is well above the maximum of the d band density of states. Figure 13 shows the local density of states of a Si impurity in a Pd matrix, broadened by a 2 eV gaussian width function. The unbroadened histogram is a cluster calculation (Terakura), and the Fermi energy is that of amorphous $Pd_{81}Si_{19}$.

F. Virtual D Band In The Hybridized Model

The presence of cobalt in the alloys implies the possible formation of local moments by the more magnetic cobalt atoms. The shape of the virtual d band is very important, as broader d states are less likely to form local moments than narrow ones. The

symmetrized d orbital density of states in the Anderson model has the form:

$$N_d(E) = N_d^0(E) \cdot \frac{1}{\pi} \frac{\Gamma(E)}{(E - E_d - \Delta(E))^2 + \Gamma^2(E)}$$

Terakura has calculated the broadening of the d orbital local density of states as a function of the impurity potential V_0. The results of the calculations, seen in Fig. 14, show that the deeper impurity potentials actually induce less broadening than the shallow potentials. The change of the Fermi level associated with the impurity is a function of both the concentration and the strength of the impurity potential. Thus, a balance occurs for the probable formation of local moments, a deeper potential causes less broadening of the d states, but the higher valence impurity shifts the Fermi energy more rapidly. The first would tend to keep $N_d(E_f)$ large, while the second would reduce its value.

Consider the case of cobalt in EL and EP NiCoP amorphous alloys. For a particular concentration of phosphorus, the Fermi level would be about the same in either phase, but the broadening of the virtual cobalt d band could be influenced by the change in the density between the phases. In general one expects lower density materials to have narrow energy bands, since in the limit of low density, the energy bands reduce to the atomic state energies. The degree of narrowing need not be severe to meet the conditions

for local moment formation, as cobalt is a more magnetic atom than nickel in these alloys. The energy bands in the low density phase of the alloy should be narrowed. An equivalent view would be to consider the impurity potential to have a slightly deeper effective potential.

G. Amorphous Hybridized Band Model (AHBM)

Application of Terakura's theoretical approach to amorphous transition metal phosphorus alloys is possible if one makes certain simplifying assumptions. It would not be correct to expect the nickel nearest neighbors to contribute as precisely as in the crystalline model; however, by averaging the contributions from the amorphous material, the results can be made similar by adjusting for the amorphous bond distances and volumes per atom in the alloy.

It has been noted that the RDF data for the EL material showed the same Ni-Ni nearest neighbor distance as that found for EP material. If this result is accurate it would seem to indicate that the difference between the two phases is subtle. Binary models consider the amorphous alloy's structure to be a close packed arrangement of nickel polyhedra, with the metalloid atoms occupying larger voids in the nickel structure. Reduction of the density through a change in structure which left the Ni-Ni nearest neighbor distance constant could be accomplished by several means. It

is possible that distortion of the Ni-Ni bonds angles in the polyhedra could produce such a volume expansion or the average number of nickel nearest neighbors of a phosphorus atom increases in the lower density material so that the phosphorus occupies a larger void in a larger nickel polyhedral arrangement. Whether either of these is close to the truth is impossible to ascertain at this time, but it is interesting to note that both put the extra volume into the voids of the polyhedral structures. It is also possible that the volume change could be due to the increase in the number of vacancies in the material. Removal of a few percent of nickel atoms from amorphous EP $Ni_{80}P_{20}$ would leave an amorphous alloy of proper density and RDF parameters for EL material at the new composition. Whatever the reason for the change in density, the effect upon the phosphorus electrons states could be considerable. In changing from the high to the low density phase the electrons at the phosphorus site would experience a reduced screening of the ion core, a reduced repulsion from electrons at the nickel site, and a change in the Fermi energy, among other things. All the above would imply a change in the phosphorus valence band density of states.

In Terakura's cluster calculations[36,37] the change in the hybridized DOS would be calculated by inserting new physical parameters such as the number and position of the near neighbors. The structural change in the lower density material should result in a reduction in the admixture between the phosphorus and nickel electron states.[39] This would cause the peak position, E_p to shift

toward the nickel d band as:

$$E_p = E_d + \Delta(E) + \Gamma(E)/q(E)$$

where:

$$\Gamma = \pi \sum_k |V_{dk}^2| \delta(E-E_k)$$

$$\Delta = \mathcal{P} \sum_k |V_{dk}^2|/E-E_k$$

The shift of the peak position toward the nickel d band can be approximated by assuming that the effective impurity potential is slightly deepened, that is, if

$$|V_{dk}^2|_{EL} < |V_{dk}^2|_{EP}$$

then the effective potential for EL material is greater than that for EP material. The nearly constant value of the "dip" position E_a, and the calculated potential dependence of E_p in Terakura's calculations allows one to determine at least two points in the new hybridized DOS.

A muffin tin potential representing phosphorus in the EP alloy can be chosen by noting that the Knight Shift results show no indication of negative polarization in the NiP alloys.[1] In Terakura's FCC nickel cluster model[37] the Vo = 1.0 Rydberg potential is the best choice as the value of $\bar{S}_L(E_f)$ is positive near the Fermi energy expected for the amorphous alloy at the ferromagnetic transition point. This choice is arbitrary as Terakura's

cluster is an FCC lattic about a substitutional impurity, but the energy dependence of the hybridized DOS in the amorphous material should be similar. The value of V_{Eff} is similarly vague, but for purposes of demonstration will be taken to be $V_{Eff} = Vo + \delta V \cong 1.1$ Rydberg. The approximate height and position of the new hybridized band can then be found, and it is known that the curve for the new hybridized DOS joins smoothly at E_a and E_p. The full curve for the hybridized DOS can then be drawn and would have a form similar to the hybridized DOS for the Vo = 1.0 Rydberg potential.

The two hybridized band curves, shown in Fig. 15, are designated N_L^+ and N_L^0, and can be used to generate a series of susceptibility curves, if it is assumed that the original unhybridized bands are equivalent. For V_0 values near one Rydberg, the original unhybridized bands are almost the same, and therefore the last assumption is not severe. The susceptibility of the hybridized band for V_0 = 1.0 Rydberg is taken to be constant, with an enhancement factor sufficient to yield a susceptibility equal to the value of $N_L^0(E)_{maximum}$. Such a susceptibility is similar to the Knight Shift results for electroplated $Ni_{1-x}P_x$ amorphous alloys.[1] This procedure yields an energy dependent enhancement factor which can then be used to solve for the modeled susceptibility of the other material. The maximum in $N_L^0(E)$ occurs at about .925 Rydberg, therefore the modeled enhancement factors can be found from:

$$S_d^0(E_f) = \frac{N_L^0(.925\ \text{Ryd.}) - N_0(E)}{N_L^0(E) - N_0(E)}$$

Inherent in this extrapolation procedure is the assumption that the enhancement factor, $S_d(E_f)$, is nearly the same for both materials. Such an assumption relies upon the fact that for small volume changes, there exist competing mechanisms in the enhancement term which tend to cancel. For instance, the narrowing of the d band due to a decrease in density would contrast with the dilution of the nickel atoms, thus $N_d(E_f)$ would increase in value and the overlap dependent U_{dd} would decrease in strength and the change in the enhancement factor would be small. The major causes of changes in $S_d(E_f)$ are the valence and composition of the alloying element, which are independent of the structure or phase. Support for this view of the enhancement factor can be found in the fact that both EP and EL NiP amorphous alloys have their ferromagnetic transition points at about 14% phosphorus.

The enhancement factors extracted from $N_L^o(E)$, the original hybridized DOS, are displayed in Fig. 16. The result seems consistant with the view that the change to ferromagnetic behavior is approaching at an energy just below that indicated on the diagram. When the same enhancement factors are applied to N_L^+, the resulting susceptibility is different. The more positive value of $\overline{S}_L(E_f)$ multiplied by the enhancement term shows a strong positive enhancement of the susceptibility as the energy nears the magnetic transition point. These extrapolated susceptibilities, seen in Fig. 17, are just a part of a family of such curves.

The amorphous hybridized band model has explored the changes in susceptibility which would result from small changes in the local environment of the impurity in the Terakura cluster system. The AHBM has generated susceptibilities which indicate a strong dependence upon the exchange enhancement, and remarkable senitivity to small changes in the density of states for alloys near the ferromagnetic transition concentration. In the analysis of the data, these theoretical modeled susceptibilities shall be compared to the measured values of the Knight shifts, spin lattice relaxation times, and Korringa ratios.

It should be noted that the hybridized DOS chosen to represent phosphorus in amorphous nickel phosphorus is similar to the hybridized DOS for arsenic (also a valence 5 atom) in FCC nickel which was calculated by Katayama, Terakura and Karamori using a muffin tin potential model.[40] Herman and Skillman[41] have shown that the position of the 4s level in arsenic and the 3s level in phosphorus are similar, thus the hybridized DOS of the two atoms in FCC nickel should be similar.

H. Linewidths, Spin Lattice Relaxation Time, and Korringa Ratios

There are several physical phenomena which contribute to the width of the NMR line. Over and beyond the linewidth due to apparatus itself, the major cases of the linewidth are dipolar broadening from the nuclear moments, inhomogenous broadening due to variations in the susceptibility at different nuclear sites

and broadening of the line due to the lifetime of the Zeeman states. For the case of alloys containing local moments, another term must be included to account for the RKKY oscillations of the spin density about a local moment.[26]

The dipolar width is not a field dependent quantity, and is sometimes refered to as the 'zero field width' (magnetic) when combined with the lifetime broadening term, which is usually much smaller. The other phenomena are all field dependent, and so the linewidth is generally written as;

$$\delta H^2 = \delta H_0^2 + (kH)^2 = (\text{Linewidth})^2$$

where k is the value from inhomogenous and RKKY broadening contributions.

Values for the zero order linewidth can give some indication of the structure of the material, in so far as dipolar fields are easily calculated from known structures. The temperature dependence of the linewidth yields information about the presence of local moments as the strength of a local moment is highly temperature dependent. Composition dependence of the linewidth can sometimes be related to a composition dependence of the susceptibility or Knight shift, showing the effect of inhomogenous broadening.

The lifetime of the Zeeman states yields a broadening of the resonance line of the order $\hbar/T_1$. The spin lattice relaxa-

tion time, T_1, is of great interest because it samples the individual contributions of the bands which combine to produce the susceptibility. The equations for the relaxation time are conventionally written in terms of T_1T, such that;

$$(T_1T)^{-1} \propto \sum_i \left(\beta_i N_i(E_f)\right)^2$$

where, β_i is the coupling of the electrons to the nucleus, and the summation is over the different contributing bands.

The Knight shifts and relaxation times can be combined to form the Korringa ratio. The Korringa ratio for a single band may be written as;[29]

$$K.R. = K^2 T_1 T / S = \left[\frac{\chi_e}{\chi_o} \frac{N_o(E_f)}{N_e(E_f)} \right]^2$$

$$S = \frac{\hbar \gamma_e^2}{\pi k \gamma_n^2}$$

where, S is a constant for a given nucleus.

χ_e is the susceptibility for the system (enhanced).

χ_o is the susceptibility for non-interacting electrons.

N_e is the density of states (enhanced, i.e. interacting).

N_o is the density of states for non-interacting electrons.

γ_e, γ_n are electron and nuclear gyromagnetic ratios.

k is the Boltzmann constant.

K is the Knight shift.

The choice of S insures that the ratio equals one for free electrons. In the presence of strong exchange enhancement the value of the Korringa ratio can give an indication of the strength of the enhancement. The exchange enhancement enters into the ratio through the static susceptibility, X_{00}, by way of the Knight shift, and through the dynamic susceptibility, X(q,w), from the relaxation time. The interacting electron states and the non-interacting electron states act as different band contributions to the relaxation times.

The enhanced portion of the relaxation time is due to electron-electron interactions which affect the off diagonal matrix elements present in the complex susceptibility. This is written in the form;[29]

$$(T_1 T)^{-1} = \frac{32\pi^2}{9} \gamma_n k \left\langle |\psi(0)|^2 \right\rangle \omega_0^{-1} \sum_q \chi''(q,\omega)$$

The susceptibility is summed over all values of the wave-number 'q' so as to include all the affected states at the Fermi level. A random phase approximation (RPA) description of the molecular fields leads to a form of exchange enhancement of the complex susceptibility. This approach helps to redefine the susceptibility equation to include the spin fluctuations of the complex susceptibility due to the off-diagonal matrix elements. The complex susceptibility can be written as;[29]

$$\chi''(q,\omega) = \frac{\chi_0''(q,\omega)}{\left[1 - u(q) F(q) N(E_F)\right]^2}$$

The function U(q) is the q dependent electron-electron interaction and the function F(q) is the linear response function of the electron system. The enhancement of the complex susceptibility is different from that in the static susceptibility which is written as;

$$\chi'(0,0) = \frac{\chi_0'(0,0)}{\left[1 - U(0)N(E_f)\right]}$$

The enhancement factor in the relaxation rate is different than that of the Knight shift term. The functions U(q) and F(q) decrease as q nears $2k_f$, which reduces the enhancement factor and thus the inverse relaxation time. In the transition metal phosphorus alloys the wave number, q, is nearly equal to $2k_f$ so the relaxation times are strongly affected by the q dependence of the enhancement factor. The full expression for the relaxation times in these materials should be of the form;

$$(T_1T)^{-1} = (\beta_0 N_0(E_f))^2 + (S(q,\omega))^2(\beta_{enh} N_{enh}(E_f))^2$$

while the Knight shift in the hybridized band model, written as a direct function of the susceptibility, would be;

$$K = \mu_B^2 a_s \left[N_0(E_f) + S_d(E_f)\left(N_L(E_f) - N_0(E_f)\right)\right]$$

For the case of phosphorus in NiP alloys the value of the coupling constants should be the same, so that $a_s = \beta_\phi = \beta_{enh}$, and $N_{enh} = N_L - N_O$. The value of the constant S is $1.603*10^{-6}$ for phosphorus atoms. Because of a lack of knowledge about the values for the q dependent functions U(q) and F(q), the concentration dependence of the relaxation times and the Korringa ratios is difficult to predict. However, at high phosphorus concentrations the enhancement factors should both reduce to their lower limit value of 1.0. For the bands shown in the previous section, the Korringa ratios may be calculated. The AHBM predicts that the ratio for these modeled bands, at a Fermi energy of about .9 Rydberg, should be about;

$$K.R. = \frac{[N_o + (N_L - N_o)]^2}{N_o^2 + (N_L - N_o)^2} \cong 2.0$$

The AHBM densities of states at high Fermi energies (i.e. high phosphorus levels) can be used to predict the ratios between the relaxation times of the modeled bands. At the peaks of the bands the ratios of the relaxation times would be approximately 1.2 to 1.0 for the adjacent bands, with the N^+ band having the smallest relaxation time. In the data analysis section these predicted relationships from the AHBM will be compared to the actual results for the Korringa ratios, the Knight shifts and the relaxation times.

IV. DATA AND DATA ANALYSIS

The physical density variation, which characterizes the difference between the EL and higher density EP material, is displayed in Fig. 18. At a given phosphorus concentration the density difference between the two types of material is about 3 percent. The ternary samples of NiCoP show densities which correspond to their binary analogs, indicating that the cobalt atoms substitute readily for the nickel atoms without a change in the structure of the material.

Very thin EL deposited samples of NiP at about 25% phosphorus seemed to show a change to EP-like densities. The large errors induced by the low weight (.1 gram) of the samples reduces the significance of this result. Since the preparation of high phosphorus concentration EL samples is difficult, attempts to further investigate the apparant trend were not pursued.

The binary alloy data fall into two catagories, the old and incomplete results of the early work[1] and the more extensive data recently aquired. With only small exceptions the older data are consistent with the new, but in the old data there is an interesting result in the Knight shift and linewidth results for low phosphorus concentration EP NiP samples. The Knight shifts and linewidths in the older samples showed a temperature dependence which

seemed to be due to the presence of local moments. It is possible that the samples were inhomogeneous, and that the temperature and composition dependence of the results was due to the presence of nickel clusters which were capable of forming local moments. This result lead us to wonder about local moment formation in the amorphous alloys, and brought about the preparation and NMR study of the NiCoP alloys.

Data collected from the more complete set of binary samples can be seen in figures 19 through 22. The Knight shift data for the EP NiP samples reproduces that of the older results. However, at the lowest phosphorus concentration studied, a $Ni_{86}P_{14}$ sample had a Knight shift of about .19% at room temperature and about .18% at 77°K. At the highest phosphorus concentration studied, a $Ni_{71.5}P_{28.5}$ sample showed Knight shifts of .134% at room temperature and of .128% at 77°K. This last sample was annealed, and found to be either crystalline $Ni_{12}P_5$ or a mixed phase of Ni_7P_3 and Ni_5P_2. The Knight shift for the annealed sample was .106% at room temperature and .084% at 77°K. These values closely correspond to the listed values for $Ni_{12}P_5$.[25] All the other EP samples had Knight shifts of between .148% and .158% at room temperature and between .138% and .148% at 77°K. The nearly constant value of the Knight shift of EP samples is sharply contrasted by the concentration dependence of the EL NiP samples. At 14% phosphorus the value of the Knight shift is between .27% and .30%, while at 25.5% phosphorus the EL sample has a Knight shift of .163%, nearly the same as that of an EP binary sample.

It should be noted that the EL and EP samples had similar temperature dependences, for example, an EL sample of $Ni_{81}P_{19}$ having K = .205% at room temperature and K = .195% at 77°K.

In addition to the bulk alloys, a complete series of powder samples were prepared, and measurements were made of their Knight shifts and spin lattice relaxation times. The Knight shift results were equivilent to the powder data except that low phosphorus composition EL and NiP sample shifts varied slightly from the bulk values. This difference in shifts is especially notable for the EL $Ni_{85}P_{15}$ samples. The reason for this difference is not known, but, since these samples were also measured for spin lattice relaxation times, the result persists through the other data.

The Knight shift data can be compared to the model susceptibilities shown in Fig. 17. The match between the Knight shifts for EP samples and χ^0 is intentional. The correlation between the EL alloy data and χ^+, the positively enhanced local susceptibility, is remarkable not only for the similar shapes of the two curves, but also for the implications which can be drawn about the magnetic, electronic and structural properties of these alloys.

The χ^+ curve is the result of a narrowed hybridized band DOS, produced from an effective potential slightly deeper than the original potential. This was done in an attempt to model the change in the hybridized DOS brought about by a reduction in the s-d admixture, a reduction which was assumed to be a direct result of a structural change characterized by the change in physical density.

The results also imply that there is significant exchange enhancement term present in both types of alloy. The sudden rise in the Knight shift of the EP $Ni_{86}P_{14}$ sample can be related to the expected composition dependence of the enhancement factor and the modeled density of states. The change in the hybridized DOS is nearly linear as the composition approaches the ferromagnetic transition point, but the enhancement factor is non-linear, rising rapidly toward its maximum value as it approaches the singularity. Therefore the change in the Knight shift would appear to be due to the dominance of the enhancement term as the alloy concentration approaches the transition point. It should be noted that the EP $Ni_{86}P_{14}$ sample was prepared after the theory indicated that the enhancement factor would dominate the local susceptibility near the ferromagnetic transition point. Thus, the results seem to be consistent with the predictions of the amorphous hybridized band model.

The linewidth results, shown in Fig. 20, are for room temperature measurements of EL and EP NiP samples. At low temperature the line is slightly broadened. Both powder and bulk measurements are included in the data, and though there are some discrepancies between them, the two sets of data are fairly consistent. The primary region of interest is again at low phosphorus concentrations, where the linewidths show features similar to those seen in the Knight shift results. In both phases of the alloy there is a rapid increase in the peak-to-peak linewidth when the alloy composition reaches $Ni_{86}P_{14}$. The most obvious conclusion is that a major part

of the linewidth is due to inhomogeneous broadening, which causes the phosphorus nuclei to sample a range of susceptibilities about the average susceptibility of the system. For a constant distribution of the positional variance of the probe nuclei, the rapidly changing susceptibility near the transition point could produce the features displayed in the linewidth graphs.

Some portion of the linewidth is due to the field independent (dipolar) broadening. Field dependent measurements of the linewidths of EL and EP $Ni_{82}P_{18}$ samples showed that the zero field linewidths were about $\delta f_{EP} \cong 1.3$ gauss, $\delta f_{EL} \cong 1.6$ gauss. Large systematic error precludes the assumption that the difference in the results is due to the phase difference in the alloys. The importance of the above results is that they are consistent with both the structural models suggested for these alloys[16,17] and the partial radial distribution functions calculated from scattering data.[7] If it is assumed that there is a random distribution of phosphorus atoms in the alloy, a dipolar width calculation from RDF data shows a zero-order linewidth approximately three times as large as the experimental value.[1] Therefore the linewidth data support the model where phosphorus has only transition metal atoms as nearest neighbors.

The results of pulsed NMR experiments which determined the spin lattice relaxation times of the resonances are displayed in Fig. 21. The EL NiP alloy data had an initial room temperature value of T_1T = .94 sec°K at 14% phosphorus. The relaxation times rise steadily to a final room temperature value of T_1T = 1.24 sec°K at 25.5% phosphorus.

Relaxation times for some samples were also measured at low temperatures of either 150^{+4}°K or 110^{+4}°K. These relaxation times had a similar composition dependence and were slightly longer than the room temperature values. The EP NiP alloy data had an initial room temperature value of $T_1T = 1.04$ sec°K at 14% phosphorus and rose to a final room temperature value of $T_1T = 1.60$ sec°K at 26% phosphorus. As was true for the EL samples, the low temperature relaxation times were all slightly longer than the room temperature values. The room temperature relaxation times of the EP and EL ternary alloys were close to the values of their binary analogs, and also showed the same temperature dependence.

For a given compositions, the EP alloy T_1T's are all longer than the EL alloy T_1T's, a result which is consistent with the hybridized band model and the apparent difference in the densities of states. In the theoretical discussion of the relaxation times, the equation for $(T_1T)^{-1}$ was written:

$$(T_1T)^{-1} \propto (a_s N_0(E_s))^2 + \left(S_d(q,\omega)\right)\left(a_s\right)\left(N_L(E_f) - N_0(E_s)\right)^2$$

For high phosphorus concentrations and Fermi energies, the value of the static susceptibility exchange enhancement factors should reduce to the lower limit value of 1.0. Therefore $S_d(q,w)$ should also reduce to 1.0 and the relaxation times should be a direct reflection of the components in the densities of states. At a Fermi energy of E_F = .925 Rydberg the modeled hybridized DOS curves were

used to calculate a ratio of the expected relaxation times for the two systems. The ratio was found to be about 1.2 to 1.0, with the low density material having the lower T_1T. The measured ratio of the EL and EP NiP alloy relaxation times at 24% phosphorus is 1.5 to 1.2, for an experimental T_1T ratio of 1.25. Once again the results are very close to the predicted values from the hybridized band model.

The Korringa ratios for the EL and EP NiP alloys are shown in Fig. 22. The EP samples have a Korringa ratio of about 2.0 throughout the composition range. Only at 14% phosphorus does the graph show a higher value, corresponding to the observed change in the Knight shift at that composition. The EL alloy sample at high phosphorus concentrations has a Korringa ratio of about 2.0. This steadily rises to a final value of 4.3 at 14% phosphorus. The "dip" at 15% phosphorus may be spurious as it was caused by the unusual powder sample result at that composition. Since the T_1T values are slowly changing, it is not surprising that the Korringa ratios show a marked similarity to the Knight shift results.

At high phosphorus concentrations, both the EL and EP samples have a Korringa ratio near 2.0. This corresponds to the predicted value from the amorphous hybridized band model.

The predicted values from the amorphous hybridized band model are founded upon the assumption that the hyperfine fields, and thereby the Knight shifts and relaxation times, depend on the direct contact term and that the coupling term, a_s, can be taken

as a constant throughout the range of compositions. If the enhancement factors are equal to one, then the Korringa ratios at high phosphorus concentrations imply that the hybridized DOS is nearly double the unhybridized DOS, i.e., $N_L(E_F) = 2N_O(E_F)$.

The data shown in Fig. 23 are the Knight shift measurements of the phosphorus resonance in NiCoP electroplated (EP) alloys. By holding the phosphorus concentration constant at near 20% and varying the cobalt to nickel ratio, the response of the system to the presence of more magnetic atoms can be determined. Cobalt is a valuable tool as the structure of CoP amorphous alloys is nearly identical to that of the NiP alloys, and it is likely that the cobalt atoms substitute readily for nickel atoms without changing the physical structure of the material. Physical density measurements of the ternary alloys support this notion, showing in addition that the same density variation between the phases persists in the ternary alloys.

The most interesting thing about the results shown in Fig. 23 is that the Knight shift remained constant as the cobalt concentration increased up to the ferromagnetic transition concentration, which occurs at about $Ni_{67}Co_{13}P_{20}$. The constant value of the Knight shift obviously indicates that for the EP phase the cobalt substitutes for the nickel without change in the system.

The linewidth data, seen in Fig. 24, shows a slowly increasing peak to peak linewidth as the cobalt concentration is increased up to 12% cobalt. This result is consistent with the additional nearest neighbor dipole moments introduced by the spin 7/2 cobalt nuclei.

There is no evidence of local moment formation and also no indication that the cobalt causes any change in the hybridized valance band density of states.

The NMR data showed a dramatic change when the same experiments were performed in the lower density EL phase. It is apparent that the Knight shift is constant up to about 6% cobalt, as can be seen in Fig. 25. After this point the increasing cobalt concentration began to show an effect upon the data which was apparently due to the formation of local moments. The Knight shift dropped and became more temperature dependent, and the linewidth broadened and showed a strong temperature dependence. The strength of the effect grew as the cobalt concentration was increased to the limit of the ferromagnetic transition concentration at about 13% cobalt. Figures 26 and 27 show the linewidth data and the temperature dependence of the linewidth as a function of the cobalt concentration.

These results are consistent with the changes caused by the formation of local moments, that is, a negative shift of the resonance and a broadening of the lineshape caused by the RKKY oscillations of the spin density as explained in the theory section. The composition dependence of the Knight shift and relaxation times shows that increasing the cobalt concentration increases the strength of the local moments and their temperature dependent behavior. These results exactly correspond to the situation seen for the case of impurities which form local moments in the noble metals.[26,28,31]

The data in figures 28 and 29 shows the temperature dependence of the Knight shift and linewidth of the EL $Ni_{70.6}Co_{8.4}P_{21}$ sample, displaying the results at room temperature, 77°K, and at the temperature of liquid helium, 4°K. The large changes at 4°K clearly demonstrate the increasing strength of the effect as the temperature of the sample is reduced. This is in keeping with the behavior of a local moment system, in which the magnitude of the moment is increased as the temperature is lowered.[30]

The final data section deals with alloys of the form $Ni_xCo_{6.0}P_y$, where the interest is upon the effect of varying phosphorus content while holding the cobalt content constant. The results for EP alloys of the form $Ni_xCo_{6.75}P_y$ are similar to the binary data, that is, the cobalt does not change the Knight shift from the binary result, and the linewidth slightly broadens due to the presence of the cobalt nuclear spins. The EL phase alloy results seen in figures 30 and 31, show that the strength of the local moment is dependent upon phosphorus concentration. At 24% phosphorus the results show no variation from the Knight shift results in the binary EL material. At 20% phosphorus the Knight shift and linewidth begin to show the changes attributed to local moment formation, and at 18% the effects due to local moment formation are increased. The implication is that at high phosphorus concentrations the moments are not formed, but as the Fermi energy drops the local density of cobalt d states at the Fermi surface increases, increasing the probability of splitting of the d states and of forming local moments.

Two methods can produce the high density phase in NiP amorphous alloys, electroplating and annealing from the EL phase. When an EL sample is annealed at moderate temperatures for fairly long times the structure of the material changes to the higher density phase. The moderate temperatures are apparently sufficient to give the constituent atoms some mobility, enough to collapse the structure but insufficient to casue full crystallization of the alloy.

Samples of EL $Ni_{1-x}P_x$ (where x = .14, .17, .195, .21) were annealed at temperatures of 230°C to 250°C for periods up to 48 hours. The new material is a mixed phase of crystallites of nickel and high density phase amorphous NiP. The nickel crystalites were disolved in a chromic-hydrosulfuric acid etch, which did not appear to affect the chemically resistant NiP amorphous alloy while disolving the nickel. Following the etch, the remnant material yielded Knight shifts and linewidths of EP type material. An EL $Ni_{86}P_{14}$ sample was annealed, and, following the etch, the physical density was measured and found to correspond to the value found for high density $Ni_{86}P_{14}$.

Rapid high temperature annealing also reveals some differences between the EL and EP amorphous alloys crystallization processes. The samples were placed in an oven at about 450°C and annealed in steps of about 5 minutes. Following the annealing, X-ray diffraction scans showed that the EL NiP alloy produced an initial step containing either $Ni_{12}P_5$ or a mixture of Ni_7P_3 and Ni_5P_2, and that the EP NiP alloy process went directly to the Ni_3P crystalline material. With continued annealing the EL sample also arrives at the final crystalline mixture of Ni and Ni_3P.

Both of the annealing experiments support the identification of the EP and EL alloys as metastable phases, with the EP alloys having a more stable structure than the EL materials.

In addition to the NMR data already presented, it is pertinent to note some related experimental results. Most important are the ^{31}P NMR measurements from other researchers' work on NiP amorphous alloys and on NiPdP and NiPtP amorphous alloys.

Bakonyi, et al.,[46] have measured the Knight shifts of ^{31}P nuclei in electroplated, electrolessly deposited and splat cooled NiP samples. Their Knight shift results generally conform to the El NiP amorphous alloy results already presented. Their EP samples appear to have Knight shifts characteristic of low density material. Perhaps this unusual result may be understood in light of Bennett's[44] investigation of pulse electroplated NiP amorphous alloys. He found that these EP alloys have the physical properties of low density material.

Hines, et al.,[45] measured the ^{31}P Knight shift in NiPdP and NiPtP splat cooled samples. The Knight shifts, spin lattice relaxation times and Korringa ratios of ^{31}P nuclei in $(Ni_{.5}Pd_{.5})_{80}P_{20}$ are nearly identical to the EL NiP alloy results already presented. NMR measurements in $(Ni_yPd_{1-y})_{80}P_{20}$ (where $.20 \leq y \leq .80$) and $(Ni_xPt_{1-x})_{75}P_{25}$ (where $.20 \leq x \leq .68$) amorphous alloys show no dependence upon the transition metal composition, reminicient of the results for the EP NiCoP alloys.

It appears that these alloys have an EL-like hybridized DOS, and that palladium and platinum atoms substitute freely for nickel atoms without changing the local environment at the phosphorus site. The substitution should not greatly change the d band DOS in these alloys, but the larger radii should increase probability for a more disordered, less dense type of structure. Extrapolation of the ternary alloy RDF data supports the idea that EP NiP alloys have a distinctly different local environment, as the extrapolated data points are inconsistent with those measured from EP NiP amorphous alloys.

V. CONCLUSIONS

The experimental results suggest that two metastable phases exist for NiP and NiCoP alloys. These structural phases are characterized by the differing physical densities and annealing behaviors of the two types of material. The EL amorphous alloys appear to be related to a group of amorphous alloys which share similar NMR and physical properties. The higher density EP amorphous alloys have unique NMR properties which suggests that the physical structure of EP alloys may also be unique.

The hybridization theory of K. Terakura has been presented and incorporated into an amorphous hybridized band model. This model was used to show the changes in the hybridized valence band for small changes in the hybridization character or potential of the metalloid atoms.

The hybridized density of states difference between the two phases could be due to difference in the admixture between the phosphorus and nickel electron states. A graphical and numerical method was used to generate a hybridized valence band density of states and modeled susceptibilities. These were used to predict the expected behavior of the Knight shifts, relaxation times and Korringa ratios for the alloys. These predictions successfully showed the trend of the EL and EP alloy data. The Knight shift was

taken to be due to the direct contact term. In the hybridized model this is written:

$$K = a_s \mu_b^2 \left[N_0(E_f) + S_d(E_f)\left(N_L(E_f) - N_0(E_f)\right)\right]$$

The model also supplied a possible reason for the apparent local moment behavior discovered in NiCoP alloys. Subsequent examination of the data showed that the onset of local moment behavior occurs at a critical cobalt concentration for a given phosphorus concentration and continues with increasing strength as the cobalt level is increased. The onset of ferromagnetism was found to be nearly identical in both types of alloys, and was interpreted as an indication that the exchange enhancement factor in both phases is similar for a given composition. The theoretical model suggested that the reason for the local moment formation was a narrowing of the cobalt d band resulting from a change in the phosphorus electron states and the narrowing expected for any state in a lower density solid.

The addition of cobalt did not appear to effect the hybridized bands or local susceptibilities in the alloys except when the local moments were formed. Cobalt seems to substitute readily for nickel, without significant change in the observed density for either type of material.

TABLE 1

Sample	R_{nn}(Å)
$Ni_{100-x}P_x$	
x = 19	2.544
x = 21	2.547
x = 23	2.560
x = 24	2.565
x = 26	2.567
$Co_{78}P_{22}$	2.58
$(Ni_{.50}Pd_{.50})_{100-x}P_x$	
x = 15	2.75
x = 17	2.75
x = 20	2.77
x = 24	2.80
x = 26.5	2.78
x = 27.5	2.77

TABLE 2

Atom of Origin	Near Neighbor	R(Å)	n
Co	Co	2.54	10.1
Co	P	2.32	2.09
P	Co	2.32	8.9
P	P	3.34	-

TABLE 3

Atom of Origin	Near Neighbor	R(Å)	n
Ni	Ni	2.55	10.7
Ni	P	2.34	2.2
P	Ni	2.34	8.5
P	P	3.30	3.6

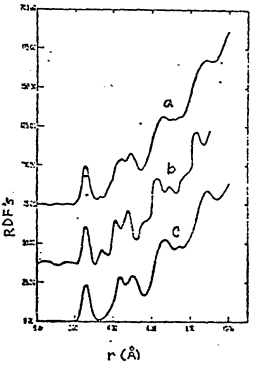

Figure 1

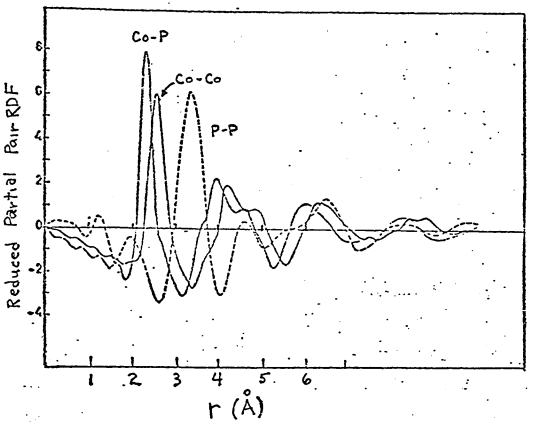

Figure 2

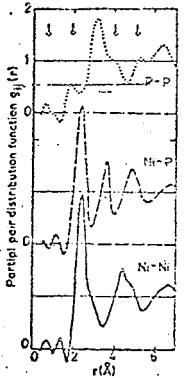

Figure 3

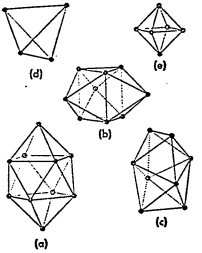

Figure 4

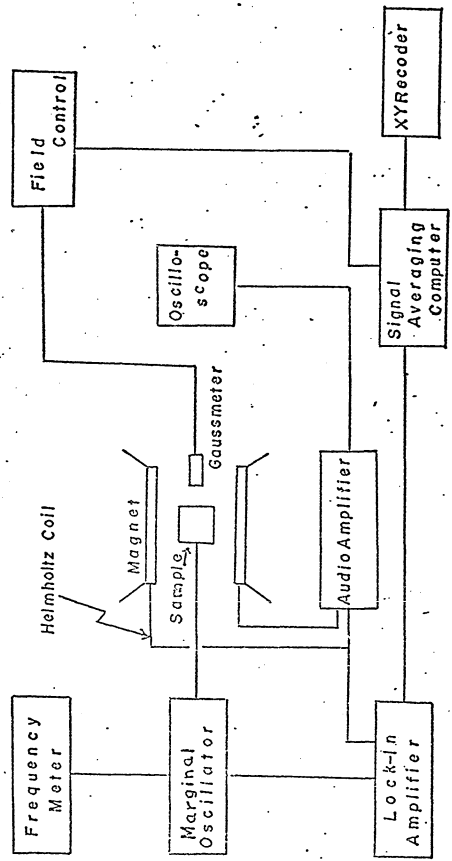

Figure 5

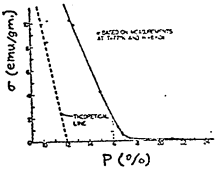

Figure 6

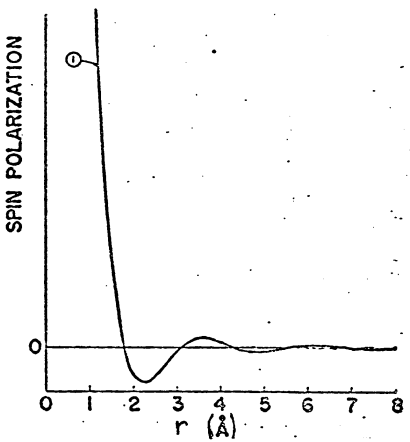

Figure 7

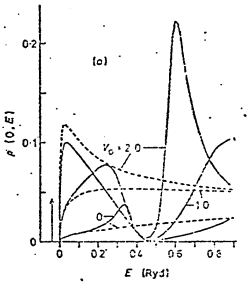

Figure 8

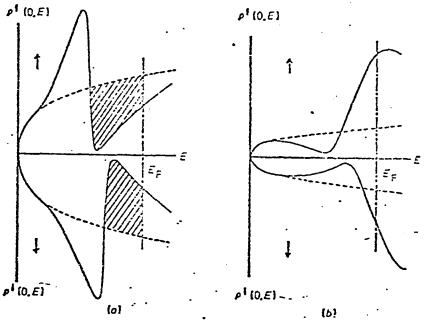

Figure 9

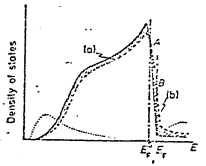

Figure 10

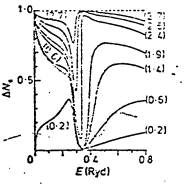

Figure 11

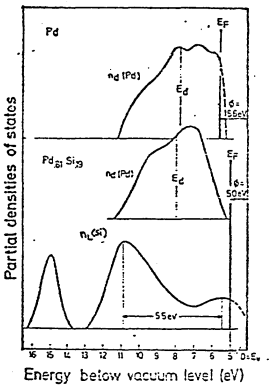

Figure 12

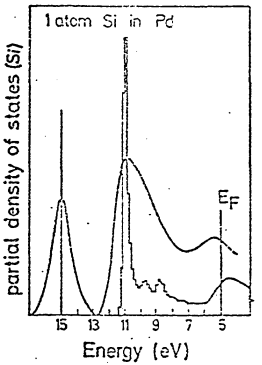

Figure 13

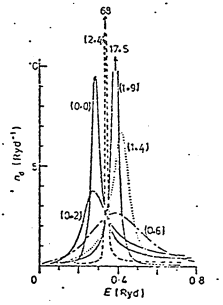

Figure 14

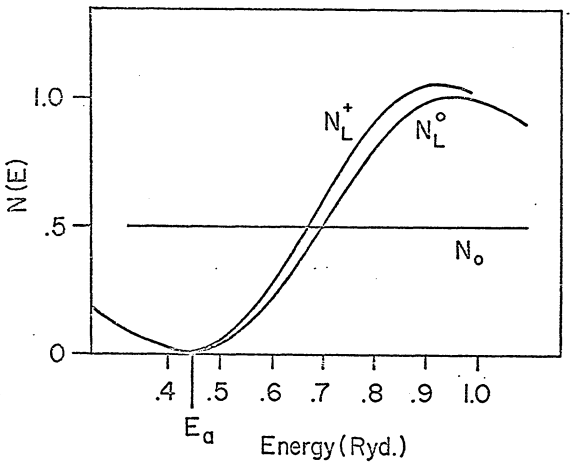

Figure 15

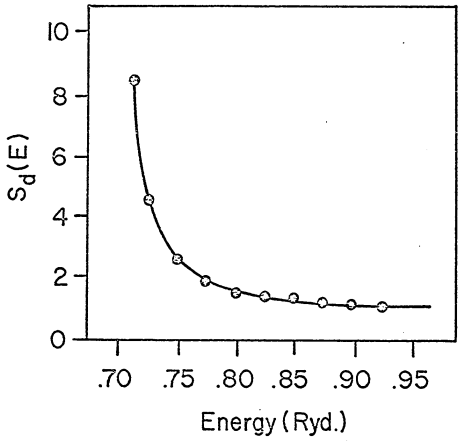

Figure 16

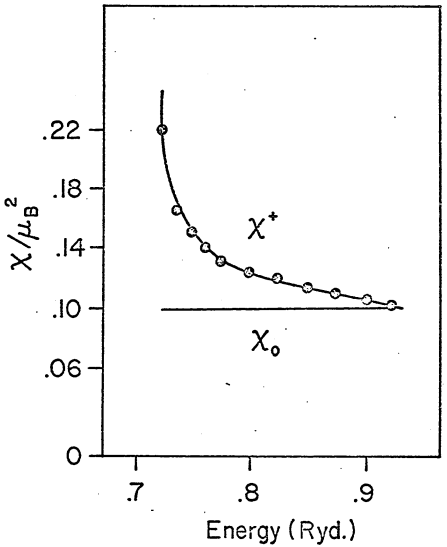

Figure 17

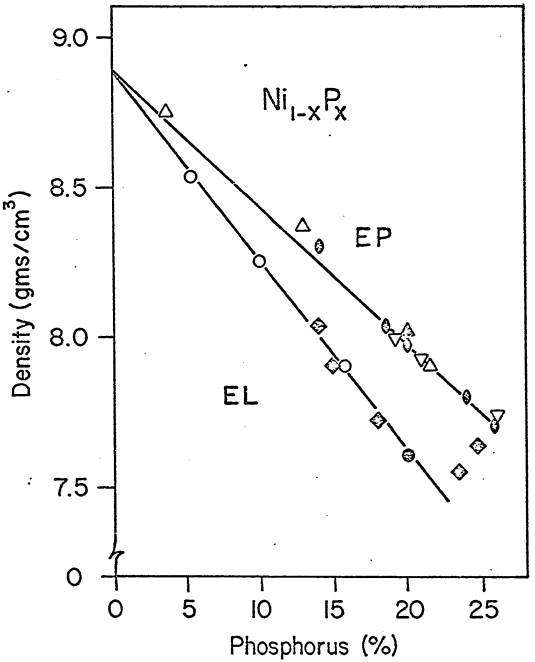

Figure 18

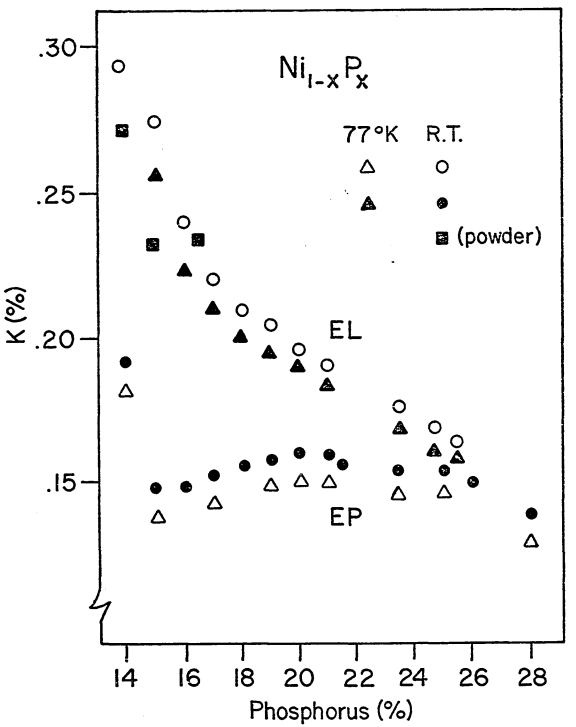

Figure 19

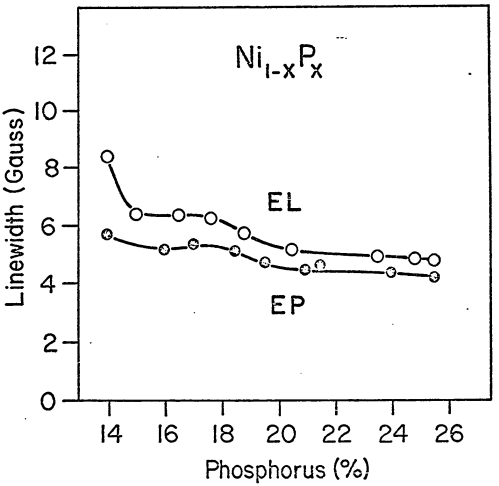

Figure 20

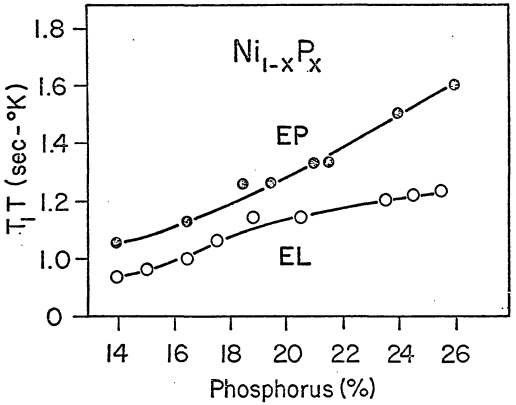

Figure 21

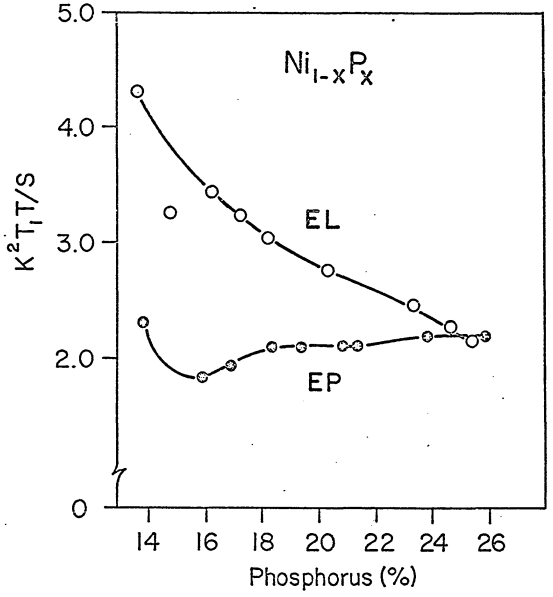

Figure 22

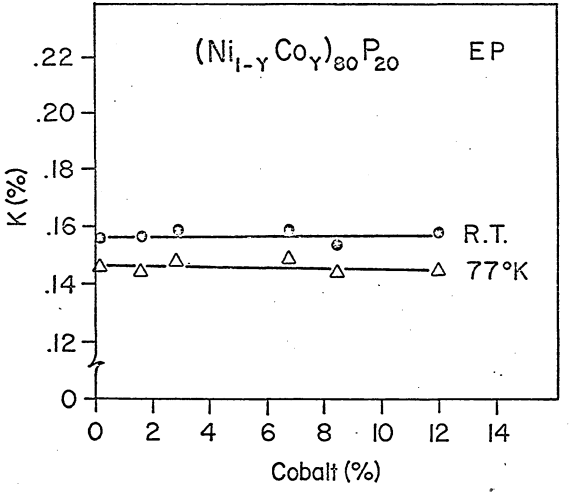

Figure 23

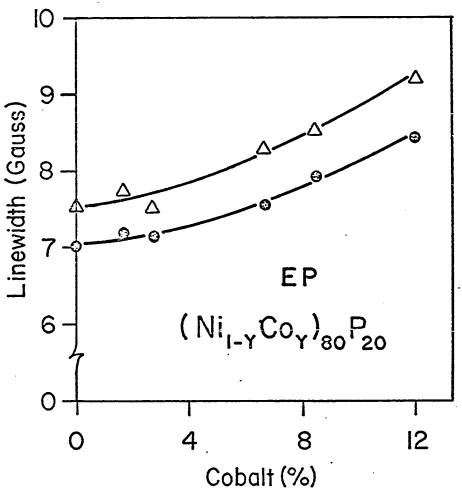

Figure 24

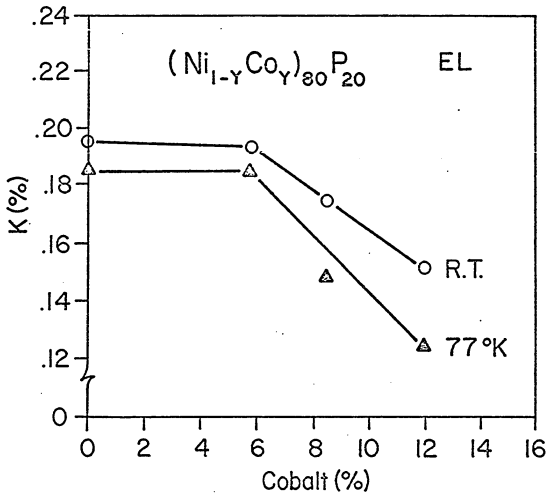

Figure 25

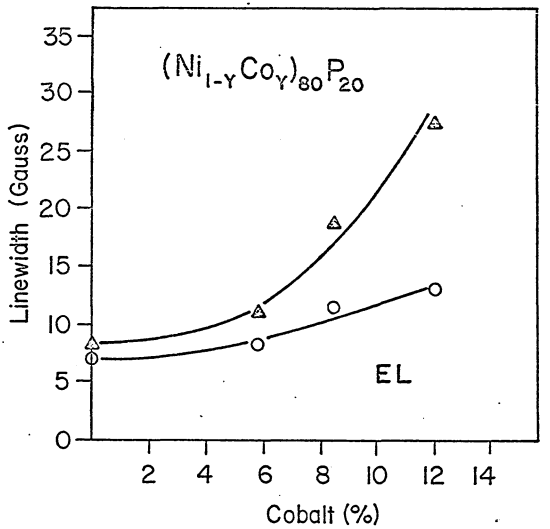

Figure 26

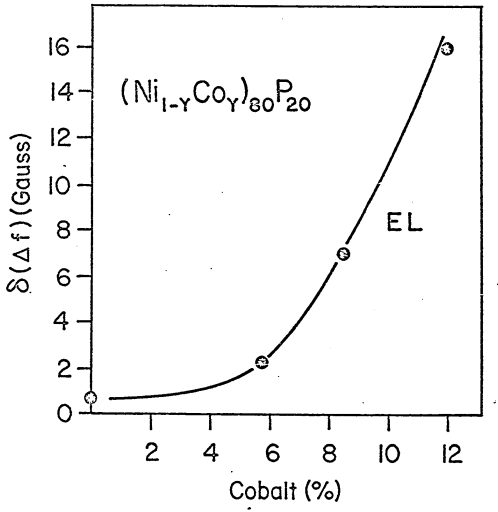

Figure 27

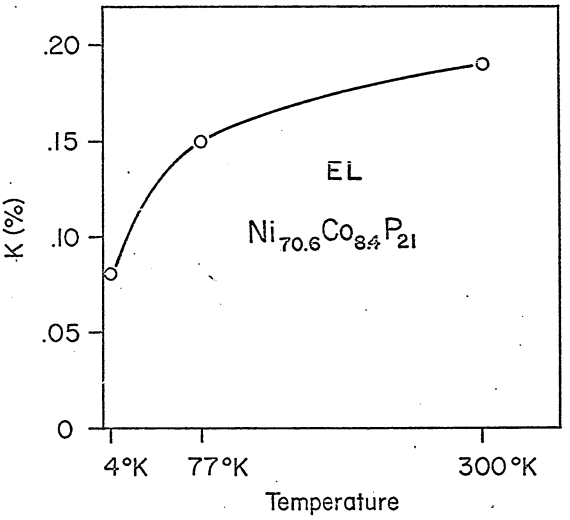

Figure 28

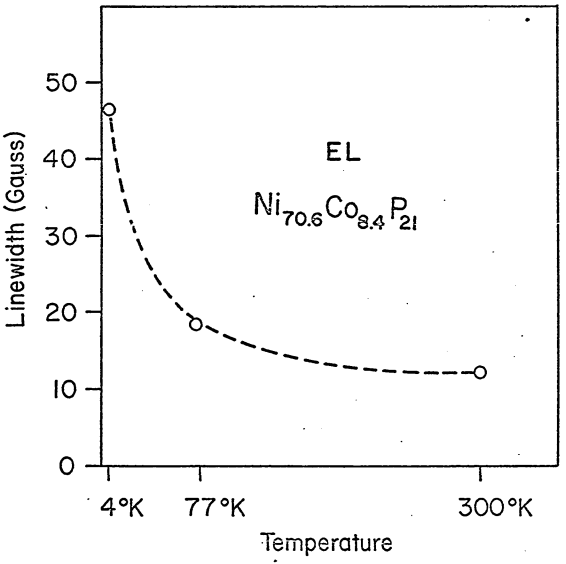

Figure 29

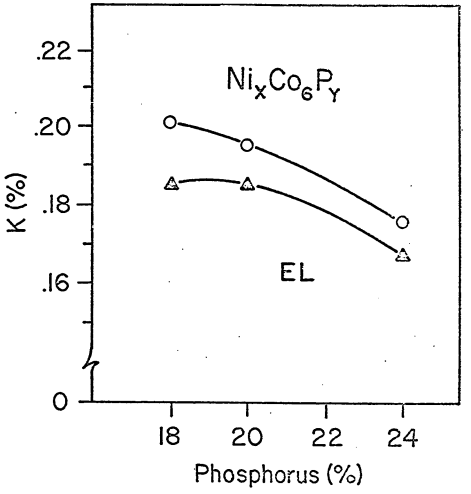

Figure 30

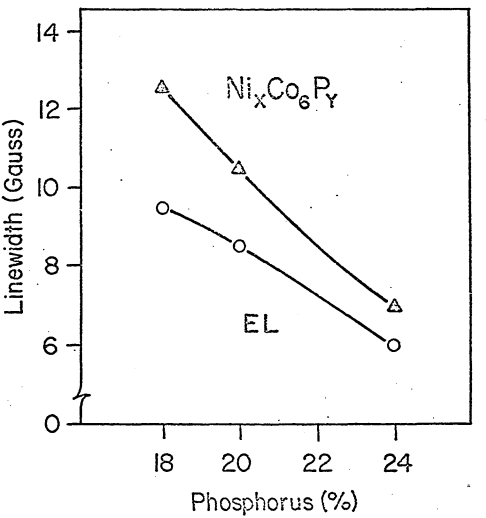

Figure 31

REFERENCES

1. H. E. Schone, P. Gustafson and L. H. Bennett, Phys. Rev. B18, 2027 (1978).
2. A. Brenner, J. Res. N. B. S., 39 (5) (1974).
3. Registered trademark, Allied Chemical Company.
4. R. D. Eng., E. J. Ryan and J. R. Doyle, Welding Journal, Oct. 1977.
5. N. DeCristofano and C. Henschel, Welding Journal, July 1978.
6. J. J. Gilman, Physics Today 28, No. 5, p. 46 (1975).
7. Y. Waseda, H. Okazaki and T. Masumoto, J. Mat. Sci. 12, p. 1929 (1977).
8. W. H. Safranek, "The Properties of Electroplated Metals and Alloys" Chap. 22, p. 465 (Elsevier, Amsterdam, 1974).
9. G. S. Cargill, III, "Advances in Solid State Physics", Vol. 30, Academic Press, (Seitz and Turnbull, eds. 1975).
10. J. Bletry and J. F. Sadoc, J. Phy. F. Metal Physics, 5 (1975), L110.
11. G. S. Cargill, III, Private Communication.
12. J. L. Finney, Proc. Roy. Soc., A, ser. A319, 495, (1970).
13. C. H. Bennett, J. Appl. Phys. 43, 2727, (1972).
14. J. F. Sadoc, J. Dixmier and A. Guinier, J. Non-Crystalline Solids 12, 46, (1973).
15. J. D. Bernal, in "Liquids: Structure, Properties, and Solid Interactions" (Elsevier, Amsterdam, 1965).

16. D. E. Polk, Acta. Met. 20, 485, (1972).

17. D. E. Polk, Scripta Met. 4, 117, (1970.

18. C. H. Bennett, D. E. Polk and D. Turnabull, Acta. Met. 19, 1295, (1971).

19. D. Turnbull, J. Phys. (Paris) 35, C4-1, (1975).

20. H. S. Chen and B. K. Park, Acta. Met. 21, 395, (1973).

21. S. R. Nagel, G. B. Fisher, J. Tauc and B. G. Bagley, Bull. Amer. Phys. Soc. 20, 374, (1975).

22. S. R. Nagel and J. Tuac, Phys. Rve. Lett. 35, 380, (1975).

23. A. Brenner, "Electrodeposition of Alloys", V. 1, Academic Press, N.Y. (1963).

24. Registered trademark, Fisher Science Corporation.

25. R. L. Parke (NBS), private communication.

26. G. C. Carter, L. H. Bennett and D. J. Kahn, in "Metallic Shifts in NMR", Prog. in Mat. Sci., vol. 20, no. 1 (1977).

27. W. D. Knight, Advances in Solid State Physics", vol. 2, p. 93, Academic Press, N. Y. (1955).

28. L. H. Bennett, R. F. Watson and G. C. Carter, "Relevence of Knight Shift Measurements to the Electronic Density of States" in Electronic Density of States, NBS Special Publication 323, (U.S. NBS Dept. of Commerce, 1971).

29. W. W. Warren, "Nuclear Magnetic Resonance in Concentrated Alloys", Bell Labs, Murray Hill, N. J. (Preprint, 1975).

30. J. M. Ziman, Principles of the Theory of Solids, sec. 10.5, (Cambridge University Press, 1972).

31. A. Narath, "Magnetic Hyperfine Interaction Studies of Magnetic Impurities in Metals", CRC Critical Reviews in Solid State Sciences, March, 1972.

32. P. W. Anderson, Phys. Rev. 124, 1, 41-51.

33. D. J. Kim, Magnetism:Selected Topics, (S. Foner, ed.) Chap. IX, (Gordon and Breach, Science Publishers, 1976).

34. Derivation by P. S. Gustafson, (1978).

35. A. Shibatani and Y. Toyozawa, J. Phys. Soc. Japan 25, 333-45, (1968).

36. K. Terakura, J. Phys. F: Metal Physics 7. no. 9, 1773 (1977).

37. K. Terakura, J. Phys. F: Metal Physics 9, no. 12, 2469 (1979).

38. R. E. Watson & A. J. Freeman, Phys. Rev. 123, 2027, (1961).

39. H. Katayama-Yosida, K. Terakura and J. Kanamori, J. Phys. Soc. Jpn. 49, no. 3, 972 (1980).

40. H. Katayama-Yosida, K. Terakura and J. Kanamori, J. Phys. Soc, Jpn. 48, 1504 (1980).

41. F. Herman and S. Skillman, Atomic Structure Calculations (Prentice Hall, N. J., 1963).

42 J. L. Beeby, Phys. Rev. 141 no. 2, 781 (1966).

43. J. D. Riley, L. Ley, F. Azouley and K. Terakura, Phys. Rev. B 20 2, 776 (1979).

44. L. H. Bennett, private communication.

45. W. A. Hines, L. T. Kabacoff, R. Hasegawa and P. Duwez, J. Appl. Phys. 49, 1724 (1978).

46. I. Bakonyi, I. Kouacs, L. Varga, T. Bagi, A. Louas, E. Toth-Kadar, and K. Tompa, Proc. Conf. Met. Glasses; (Budapest, Hungery June 30-July 4, 1980).

47. G. S. Cargill, J. Appl. Phys. 41, 12 (1970).

48. D. Pan and D. Turnbull, J. Appl. Phys. 39, 5681 (1968).

49. B. B. Schwartz, Magnetism, Selected Topics, (S. Foner, ed.) Chap. III, p. 100 (Gordon and Breach, Science Pub. Inc., 1976).